

Emerging Mesoscale Flows and Chaotic Advection in Dense Active Matter

Yann-Edwin Keta^{1,*}, Juliane U. Klamser^{1,*}, Robert L. Jack^{2,3} and Ludovic Berthier^{1,2}

¹Laboratoire Charles Coulomb (L2C), Université de Montpellier and CNRS (UMR 5221), 34095 Montpellier, France

²Yusuf Hamied Department of Chemistry, University of Cambridge, Lensfield Road, Cambridge CB2 1EW, United Kingdom

³Department of Applied Mathematics and Theoretical Physics, University of Cambridge,
Wilberforce Road, Cambridge CB3 0WA, United Kingdom



(Received 27 June 2023; revised 23 November 2023; accepted 17 April 2024; published 22 May 2024)

We study two models of overdamped self-propelled disks in two dimensions, with and without aligning interactions. Both models support active mesoscale flows, leading to chaotic advection and transport over large length scales in their homogeneous dense fluid states, away from dynamical arrest. They form streams and vortices reminiscent of multiscale flow patterns in turbulence. We show that the characteristics of these flows do not depend on the specific details of the active fluids, and result from the competition between crowding effects and persistent propulsions. This observation suggests that dense active suspensions of self-propelled particles present a type of “active turbulence” distinct from collective flows reported in other types of active systems.

DOI: 10.1103/PhysRevLett.132.218301

Active matter has emerged as an important class of nonequilibrium systems, where energy injection at single-particle level can produce emerging collective phenomena at large scales [1]. Among these, collective motion [2] is interesting because of its biological and social interest, e.g., for wound healing [3] or crowd management [4]. Collective motion can be ordered, as in flocking [5,6], where local interactions between individuals can lead to global motion along a given direction, or be more irregular or even chaotic, as in bacterial swarms [7] or active nematics [8], which display intermittent swirling motion.

Building on early results for bacterial suspensions [9–12], the term “active turbulence” [13] recently became popular to describe chaotic mesoscale flows in systems including dense epithelial tissues [14] and active suspensions of microtubules [15]. Unlike classical turbulence, active turbulence occurs in the absence of inertia. Moreover, the energy injection is not externally imposed but self-generated at small scales [13]. A recent classification [13] organizes active turbulent models into four classes, depending on their symmetries: a model’s order parameter can be either polar or nematic; it is called “wet” if it conserves momentum—for example, if hydrodynamic interactions dominate—and “dry” if it does not.

In both wet and dry nematic systems [16–18], flow derives from a dynamical instability of the nematic director

field, with an emerging length scale determined by the balance between active and nematic stresses [16,18]. Long-range velocity correlations in these flows are universal [18]. Most studies of polar active turbulence have either considered wet systems of swimmers [19], or the Toner-Tu-Swift-Hohenberg equation [10,20], which describes incompressible flows in dry systems. In this latter description, polarization and velocity are assumed to be aligned: this is appropriate in the absence of steric interactions. Diverse particle-based models have also been shown to display active turbulence: extensions of the Vicsek model [21,22], self-propelled rods [10,17,23,24] and dumbbells [25], microswimmers with hydrodynamic interactions [26,27]. All these previously studied models comply with the existing classification [13].

Here, we establish that the simplest class of active matter models—overdamped self-propelled disks—also develops mesoscale chaotic flows qualitatively similar to active turbulence; see Fig. 1. In two distinct models, we find that the homogeneous dense active fluid develops extended spatial velocity correlations [28–34] that advect particles over large distances along a disordered array of streams and vortices, accompanied by hallmarks of active turbulence, including advective mixing. Within the existing symmetry classification [13], the natural comparison is polar turbulence with dry friction [10] but our results show different scaling behavior. This is due to particle crowding, which is absent from previous descriptions of active turbulent systems. Based on these observations we argue for a new class of active turbulent behavior, which should encompass diverse models such as vibrated disks [35], self-aligning self-propelled particles [36,37], or self-propelled Voronoi models of confluent tissues [38].

Published by the American Physical Society under the terms of the Creative Commons Attribution 4.0 International license. Further distribution of this work must maintain attribution to the author(s) and the published article’s title, journal citation, and DOI.

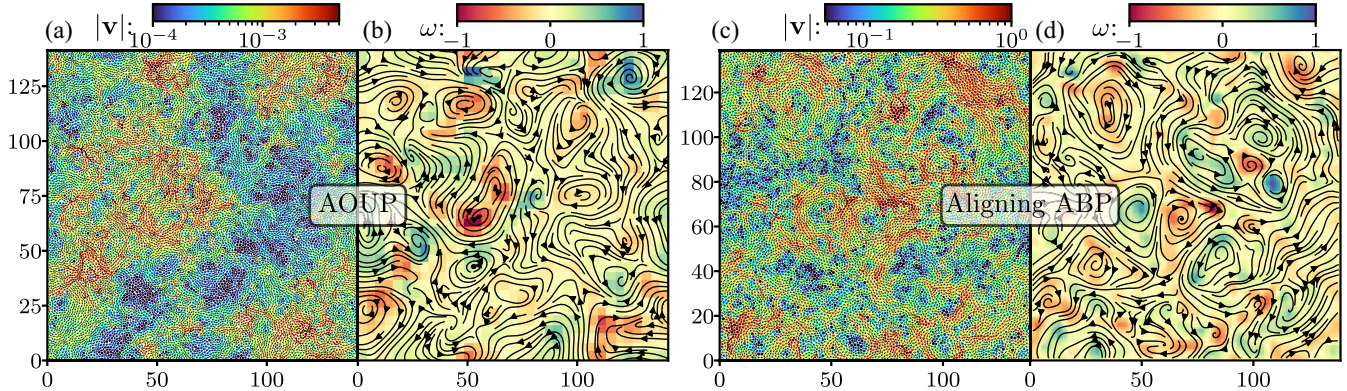


FIG. 1. (a) Configuration snapshot at $\phi = 0.8425$ of $N = 16384$ AOUPs with velocity field (arrows) and corresponding velocity amplitude (color) showing fast and slow regions of collective motion for $\tau_p = 10^4$. The corresponding vorticity field with streamlines in (b) highlights the presence of streams and vortices in the velocity field. (c),(d) Are for $N = 12800$ aligning ABPs, which show a comparable phenomenology at $\phi = 0.97$ and $\gamma = 2.5$.

We study N overdamped athermal self-propelled particles in a square $L \times L$ box with periodic boundary conditions, following overdamped dynamics:

$$\dot{\mathbf{r}}_i = -\mu \sum_{j \neq i} \nabla_i U(r_{ij}) + \mu \mathbf{p}_i, \quad (1)$$

where \mathbf{r}_i is the position of particle i , \mathbf{p}_i the self-propulsion force, μ the particle mobility, $r_{ij} = |\mathbf{r}_i - \mathbf{r}_j|$, and particles interact via a repulsive Weeks-Chandler-Andersen potential $U = 4\epsilon[(\sigma_{ij}/r_{ij})^{12} - (\sigma_{ij}/r_{ij})^6 + 1/4]$ for $r_{ij} < 2^{1/6}\sigma_{ij}$ and $U = 0$ otherwise, where $\sigma_{ij} = (\sigma_i + \sigma_j)/2$ with σ_i the diameter of particle i .

The dynamics of the self-propulsion forces \mathbf{p}_i defines the active model [39]. We considered two distinct dynamics, active Ornstein-Uhlenbeck particles (AOUPs) [40,41] and aligning active Brownian particles (ABPs) [42–45]. To frustrate positional order, we introduce size polydispersity. The diameters of the AOUPs are drawn from a uniform distribution of mean $\sigma = \bar{\sigma}_i$ and polydispersity 20% [41,46]. The ABPs are a 50:50 bidisperse mixture with diameters σ and 1.4σ . The packing fraction is $\phi = 2^{1/3}\pi N \bar{\sigma}_i^2 / (4L^2)$. The unit length is σ , the unit energy is ϵ , and the unit time is $\mu\sigma^2/\epsilon$. We measure velocities $\mathbf{v}_i = \dot{\mathbf{r}}_i - N^{-1} \sum_j \dot{\mathbf{r}}_j$ in the center-of-mass frame.

For AOUPs, the self-propulsion forces obey

$$\tau_p \dot{\mathbf{p}}_i = -\mathbf{p}_i + \sqrt{2D_0} \boldsymbol{\eta}_i, \quad (2)$$

where τ_p is the persistence time, D_0 the diffusion constant of a free particle, and $\boldsymbol{\eta}_i$ a Gaussian white noise of zero mean and unit variance, $\langle \boldsymbol{\eta}_i(t) \boldsymbol{\eta}_j(0) \rangle = \mathbb{1}_{ij} \delta(t)$. From Eq. (2), the amplitude of the self-propulsion force fluctuates around $\sqrt{\langle |\mathbf{p}_i|^2 \rangle} = \sqrt{2D_0/\tau_p}$. We use $D_0 = 1$, and vary τ_p toward large values. We use system sizes up to $N = 262144$ (depending on the state point), to ensure that

results are not significantly affected by finite size effects (see SM [47] for numerical tests).

For aligning ABPs, $\mathbf{p}_i = v_0 \mathbf{u}_i$ with a constant amplitude v_0 and orientations $\mathbf{u}_i = (\cos \theta_i, \sin \theta_i)$ evolving as

$$\dot{\theta}_i = \frac{\gamma}{n_i} \sum_{j \neq i} f(r_{ij}) \sin(\theta_j - \theta_i) + \sqrt{2D_r} \xi_i, \quad (3)$$

with γ the alignment strength, $f(r_{ij}) = 1$ if $r_{ij}/\sigma_{ij} < 2$ and zero otherwise, $n_i = \sum_{j \neq i} f(r_{ij})$ the number of particles interacting with particle i , and D_r the rotational diffusivity that controls the single-particle persistence time $\tau = D_r^{-1}$. We fix v_0 and D_r to 1, and use modest γ values, which are well below the onset of polar order. We use system sizes up to $N = 51200$.

Figure 1 illustrates the emergent flows that are the main subject of this work (see SM [47] for corresponding movies): it displays velocity (\mathbf{v}) and vorticity ($\nabla \times \mathbf{v}$, coarse-grained over a suitable length) fields, as well as streamlines. For suitable parameters, both models support homogeneous states where spatiotemporal fluctuations of the velocity field lead to mesoscale chaotic flows: these are the established features of active turbulence [13]. The patterns in Fig. 1 are highly dynamical and constantly form new networks of streams and vortices. Velocity correlations appear in these systems under a broad range of conditions (phase-separated [48], glassy [29,32], jammed [28,49], crystalline [31]). Our central finding is that homogeneous active fluids support, in addition to extended velocity correlations at large persistence, active turbulent phenomenology. This can be easily missed because the turbulence is suppressed by phase separation and by dynamical arrest (or emergence of positional order in monodisperse systems), to which dense persistent active fluids are very susceptible [41,50].

Such active turbulent phenomenology in AOUPs is surprising because there are no interactions favoring

alignment of the self-propulsion forces explicitly or via shape anisotropy. Instead, flows emerge because extended velocity correlations arise from the coupling between persistent self-propulsion and density fluctuations [31–33]. The relevant densities are large enough to avoid motility induced phase separation [51] and small enough to avoid dynamic arrest [41]. For AOUPs under these conditions, advective flows develop gradually as τ_p increases [33] [$\tau_p = 10^4$ in Figs. 1(a) and 1(b)]. This observation motivates our second model with weak alignment, in which similarly persistent self-propulsion arises from the aligning interactions, even if isolated particles decorrelate quickly ($\tau = 1$). This drives aligning ABPs toward the same turbulent behavior as highly persistent AOUPs. Strong velocity correlations emerge in both models from the interplay of crowding and very long persistence times; for the AOUPs this persistence comes from the particles themselves but for aligning ABPs it comes from the combination of a moderate D_r with an aligning interaction, which slows down the orientational relaxation.

Despite differences in microscopic details, Fig. 1 shows that the velocity correlations are almost indistinguishable in both models, as confirmed below. These quantitative similarities for systems controlled by particle crowding support our identification of a new class of active turbulent systems, whose origin is the interplay of self-propulsion and crowding. In all cases, velocity correlations are much longer-ranged than the correlations of the self-propulsion forces \mathbf{p}_i , which are either absent (AOUPs) or weak (aligning ABPs): velocity correlations are an emerging property. This situation is in contrast to the mechanism of correlated propulsions described by existing continuum theories [10], supporting our claim that these observations are not included in the current classification of active turbulent systems [13].

We now provide quantitative measurements for both velocity correlation and chaotic advective transport, supporting the above conclusions. Figures 2(a) and 2(b) show velocity autocorrelation functions, $\langle \mathbf{v}_i(0) \cdot \mathbf{v}_i(t) \rangle / \langle |\mathbf{v}|^2 \rangle$, which reveal the temporal behavior of the flows. Packing fractions ϕ are chosen so that the system does not phase separate and remains away from dynamical arrest. Unlike the exponential decay of simple fluids [52], both models show two-step decay that becomes more pronounced with more turbulent flows. These two time-scales respectively correspond to the short collision time and the increasing decorrelation time of the self-propulsion forces. In AOUPs, this longer correlation time corresponds to the persistence time τ_p ; in ABPs, it is controlled by the alignment strength γ (recall that $\tau = 1$ throughout).

We quantify spatial velocity correlations using the analog of the kinetic energy spectrum [10]

$$E(k) = \frac{2\pi}{L^2} k \langle |\tilde{\mathbf{v}}(\mathbf{k})|^2 \rangle, \quad (4)$$

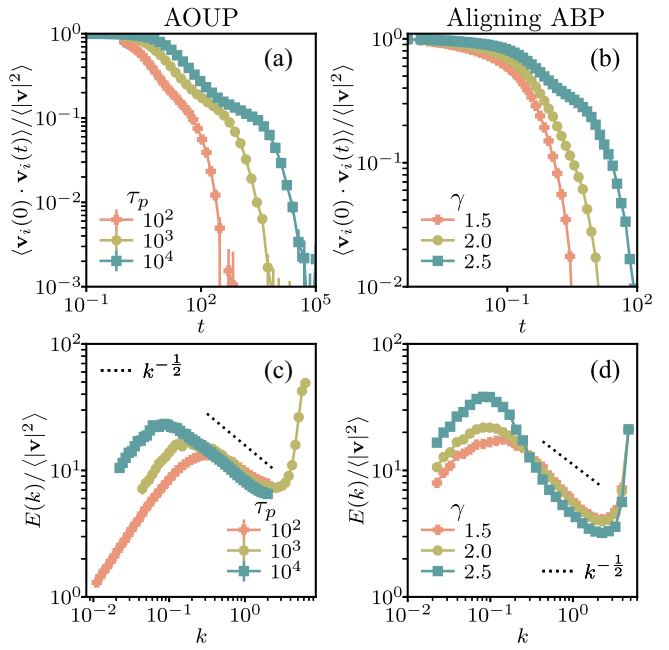


FIG. 2. (a),(b) Velocity autocorrelations in time and (c),(d) kinetic energy spectra defined in Eq. (4) for (a),(c) AOUPs at various persistence times τ_p and (b),(d) aligning ABPs for a range of alignment strengths γ . For AOUPs, $\phi = 0.84$ for $\tau_p = 10^2, 10^3$ and $\phi = 0.8425$ for $\tau_p = 10^4$. For ABPs, $\phi = 0.97$.

with $k = |\mathbf{k}|$ and $\tilde{\mathbf{v}}(\mathbf{k}) = \int d^2r \mathbf{v}(\mathbf{r}) \exp(-i\mathbf{k} \cdot \mathbf{r})$ the Fourier transform of the velocity field $\mathbf{v}(\mathbf{r}) = \sum_i \mathbf{v}_i \delta(\mathbf{r} - \mathbf{r}_i)$; see Figs. 2(c) and 2(d). Velocity correlations in real space are directly related to $E(k)$. For all parameters, $E(k) \sim k$ for small enough k , which implies the existence of a maximum length scale ξ beyond which velocities are uncorrelated, so that $\langle |\tilde{\mathbf{v}}(\mathbf{k})|^2 \rangle = \text{const}$ for $k\xi \ll 1$. This ξ is the correlation length of the velocities.

For wave vectors k intermediate between $2\pi/\xi$ and $2\pi/\sigma$, we report a decay of the energy spectrum $E(k) \propto k^{-\alpha}$ with $\alpha \approx 1/2$. This corresponds to a scale-free decay $\sim r^{\alpha-1}$ of velocity correlations for length scales between the particle size σ and the correlation length ξ [53]. Established classes [13] of active turbulent behavior involve exponents $\alpha \approx 1$ [18,19] or much larger (for example $\alpha = 8/3$ [10]). Physically, α quantifies the observation that the velocity fields in Figs. 1(a) and 1(c) display self-similar structure up to the (parameter-dependent) correlation length ξ . For systems of nonaligning self-propelled particles, previous studies [32,33,54] focusing on different parameter regimes reported results qualitatively similar to those of Fig. 2 but suggested $\alpha = 1$, consistent with hydrodynamic models of self-propulsion coupled to small density fluctuations, leading to predictions of the Ornstein-Zernike form that cannot describe our numerical results (see SM). While this discrepancy could be due to corrections to scaling in the explored numerical regime, our observations can also be interpreted as a breakdown of the assumption of small

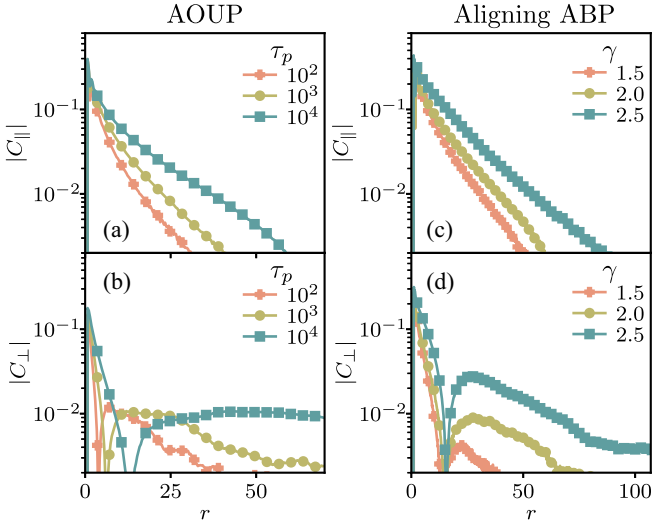


FIG. 3. Real-space velocity correlations $C_{\parallel}(r)$ and $C_{\perp}(r)$ defined in Eq. (5), for AOUPs and aligning ABPs. The correlation length in $C_{\parallel}(r)$ (a),(c) and the amplitude of negative correlations in $C_{\perp}(r)$ (b),(d) can be tuned by increasing τ_p or γ respectively. Volume fractions ϕ are as in Fig. 2.

Gaussian fluctuations in the presence of strong chaotic flows. Indeed we find that $\alpha = 1$ describes our data very well in the arrested solid regime at much larger density, where the assumptions of Ref. [32] apply.

To further characterize these flow patterns, we decompose the real-space velocity correlations into longitudinal ($\lambda = \parallel$) and transverse ($\lambda = \perp$) components:

$$C_{\lambda}(r) = \frac{\langle \sum_{i,j} v_i^{\lambda} v_j^{\lambda} \delta(r_{ij} - r) \rangle}{\langle \sum_{i,j} \delta(r_{ij} - r) \rangle}, \quad (5)$$

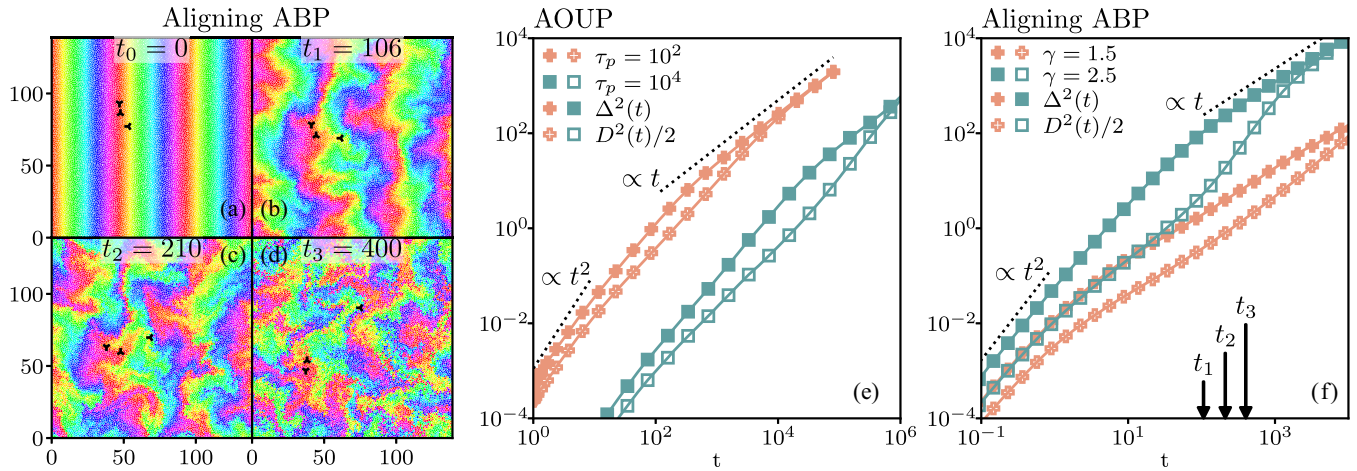


FIG. 4. (a)–(d) Time series of configurations for aligning ABPs at $\gamma = 2.5$, $\phi = 0.97$. Particles are colored according to their x position at some time in the steady state denoted $t_0 = 0$. (e),(f) Mean-squared displacement $\Delta^2(t)$ (full symbols) and mean-squared displacement difference of initially close-by particles $D^2(t)$ (open symbols) for (e) AOUPs and (f) aligning ABPs. The indicated times in (f) correspond to the snapshots in (b)–(d). Volume fractions ϕ are as in Fig. 2.

where v_i^{λ} is the velocity component in the direction parallel or transverse to the unit vector $(\mathbf{r}_i - \mathbf{r}_j)/r_{ij}$. The total velocity correlation function is $C(r) = C_{\parallel}(r) + C_{\perp}(r)$, but this decomposition is distinct from the Fourier space analysis of [32,33], where \mathbf{v} is instead resolved parallel and perpendicular to the wave vector \mathbf{k} (see SM [47] for data and finite size analysis). Figure 3 shows results in both models for a range of state points. The decomposition separates the long-ranged positive correlations along streams [in $C_{\parallel}(r)$], and the anticorrelations characteristic of vortices [in $C_{\perp}(r)$] [55]. The data confirm a similar structure for both models, and show quantitatively that velocities are correlated over tens of particle diameters for the more persistent systems, in agreement with the peak position in $E(k)$ and the snapshots in Fig. 1. The characteristic size ξ of the velocity patterns can be tuned via the persistence time τ_p of AOUPs, or the alignment strength γ of ABPs. This leads in both cases to more extended streams and vortices, together with increasing length scales in $C_{\parallel}(r)$ and $C_{\perp}(r)$. The latter two length scales do not need to grow in the same manner [33].

These emerging velocity correlations dramatically impact particle transport in these highly persistent, homogeneous fluid states. This is revealed in Fig. 4 by “dyeing” particles according to their position at some initial time t_0 in the steady state, and watching them spread over time. Transport is dominated at initial times by rapid advection along extended streams, as revealed by the initial distortion of the pattern with mutually invading branches that stretch and fold over a range of length scales, resembling chaotic advection (see times t_1 and t_2). Only at large times do particles diffuse into regions of different colors, which eventually blends the dyes. We highlight three tracer particles that are initially close, showing that particle pairs

are either advected large distances together or separated almost immediately. These time-dependent patterns are qualitatively similar to the chaotic advection created by time periodic flows [56].

We quantify these observations using the mean-squared displacement $\Delta^2(t) = \langle |\Delta\mathbf{r}_i(t)|^2 \rangle$ and the mean-squared distance between initially close-by particles (as studied in inertial turbulence [57–59]), $D^2(t) = \langle |\Delta\mathbf{r}_i(t) - \Delta\mathbf{r}_j(t)|^2 \rangle$, where $\Delta\mathbf{r}_i(t) = \mathbf{r}_i(t) - \mathbf{r}_i(0)$ and the average is restricted to nearby pairs of particles with $|\mathbf{r}_i(0) - \mathbf{r}_j(0)| < 1.15\sigma_{ij}$ [60]. By construction, both quantities vanish at $t = 0$, while $D^2 \sim 2\Delta^2 \sim t$ holds in the diffusive regime at large times (for which particles i, j eventually decorrelate); see Figs. 4(e) and 4(f).

Self-propulsion causes ballistic motion $\Delta^2 \sim t^2$ at small times. The corresponding velocity decreases significantly for AOUPs as τ_p is increased at constant D_0 , mirroring the reduction in strength of \mathbf{p}_i . In contrast, the velocity increases slightly with γ for ABPs. This ballistic regime is quickly interrupted by interparticle collisions at a corresponding very small length scale. At very large times, memory of the self-propulsion forces is lost and particles diffuse, $\Delta^2 \sim t$. Between these two limits, we observe an intermediate advective (superdiffusive) regime, which is demarcated by the two well-separated timescales found in the velocity autocorrelation function [recall Figs. 2(a) and 2(b)].

The advection is also apparent in D^2 , which is similarly ballistic at very short times. At intermediate times, D^2 grows significantly slower than Δ^2 , showing that pairs of particles can be advected together over extremely large distances, leading to $D^2 \ll \Delta^2$. Eventually, particles' memory of their initial conditions is lost: this leads to superdiffusive scaling, as D^2 "catches up" with the long-time diffusive scaling $D^2 \sim 2\Delta^2 \sim t$.

In conclusion, we established that a novel form of active turbulence generically emerges in two well-studied models of dry, isotropic, self-propelled particles. The resulting mesoscale flows should be observable in a broad range of systems; they resemble other active chaotic flows, displaying scale-free behavior from the particle size up to a correlation length scale that is easily tuned by the model parameters. While previous theoretical descriptions of active turbulence rely on either polar or nematic interactions [13], velocity correlations emerge in both our models from the competition between highly persistent forcing and crowding. The link between spontaneous spatial velocity correlations in dense active matter [32,33,48] and active turbulence [13] has been overlooked. Further work is thus needed to determine if existing theories for either of these phenomena are compatible, or if new theoretical approaches are needed. Unusual transport properties emerge from the correlated velocity fields, including chaotic advection over large distances, which directly impact mixing dynamics. Such properties

may be useful when energy sources for the active particles are localized [61], in active matter with open boundaries [3], or for mixtures of active particles [62]: all these cases deserve further study.

We thank D. Bartolo, J. Tailleur, and J. Yeomans for useful discussions. This work was publicly funded through ANR (the French National Research Agency) under the THEMA AAPG2020 grant. It was also supported by a grant from the Simons Foundation (#454933, L. B.), and by a Visiting Professorship from the Leverhulme Trust (VP1-2019-029, L. B.).

*These authors contributed equally to this work.

- [1] M. C. Marchetti, J. F. Joanny, S. Ramaswamy, T. B. Liverpool, J. Prost, M. Rao, and R. A. Simha, Hydrodynamics of soft active matter, *Rev. Mod. Phys.* **85**, 1143 (2013).
- [2] T. Vicsek and A. Zafeiris, Collective motion, *Phys. Rep.* **517**, 71 (2012).
- [3] M. Basan, J. Elgeti, E. Hannezo, W.-J. Rappel, and H. Levine, Alignment of cellular motility forces with tissue flow as a mechanism for efficient wound healing, *Proc. Natl. Acad. Sci. U.S.A.* **110**, 2452 (2013).
- [4] N. Bain and D. Bartolo, Dynamic response and hydrodynamics of polarized crowds, *Science* **363**, 46 (2019).
- [5] T. Vicsek, A. Czirók, E. Ben-Jacob, I. Cohen, and O. Shochet, Novel type of phase transition in a system of self-driven particles, *Phys. Rev. Lett.* **75**, 1226 (1995).
- [6] J. Toner and Y. Tu, Long-range order in a two-dimensional dynamical XY model: How birds fly together, *Phys. Rev. Lett.* **75**, 4326 (1995).
- [7] G. Ariel, A. Rabani, S. Benisty, J. D. Partridge, R. M. Harshey, and A. Be'er, Swarming bacteria migrate by Lévy Walk, *Nat. Commun.* **6**, 8396 (2015).
- [8] A. Doostmohammadi, J. Ignés-Mullol, J. M. Yeomans, and F. Sagués, Active nematics, *Nat. Commun.* **9**, 3246 (2018).
- [9] C. Dombrowski, L. Cisneros, S. Chatkaew, R. E. Goldstein, and J. O. Kessler, Self-concentration and large-scale coherence in bacterial dynamics, *Phys. Rev. Lett.* **93**, 098103 (2004).
- [10] H. H. Wensink, J. Dunkel, S. Heidenreich, K. Drescher, R. E. Goldstein, H. Löwen, and J. M. Yeomans, Meso-scale turbulence in living fluids, *Proc. Natl. Acad. Sci. U.S.A.* **109**, 14308 (2012).
- [11] J. Dunkel, S. Heidenreich, K. Drescher, H. H. Wensink, M. Bär, and R. E. Goldstein, Fluid dynamics of bacterial turbulence, *Phys. Rev. Lett.* **110**, 228102 (2013).
- [12] E. Lushi, H. Wioland, and R. E. Goldstein, Fluid flows created by swimming bacteria drive self-organization in confined suspensions, *Proc. Natl. Acad. Sci. U.S.A.* **111**, 9733 (2014).
- [13] R. Alert, J. Casademunt, and J.-F. Joanny, Active turbulence, *Annu. Rev. Condens. Matter Phys.* **13**, 143 (2022).
- [14] S.-Z. Lin, W.-Y. Zhang, D. Bi, B. Li, and X.-Q. Feng, Energetics of mesoscale cell turbulence in two-dimensional monolayers, *Commun. Phys.* **4**, 21 (2021).

- [15] L. M. Lemma, S. J. DeCamp, Z. You, L. Giomi, and Z. Dogic, Statistical properties of autonomous flows in 2D active nematics, *Soft Matter* **15**, 3264 (2019).
- [16] L. Giomi, Geometry and topology of turbulence in active nematics, *Phys. Rev. X* **5**, 031003 (2015).
- [17] M. Bär, R. Großmann, S. Heidenreich, and F. Peruani, Self-propelled rods: Insights and perspectives for active matter, *Annu. Rev. Condens. Matter Phys.* **11**, 441 (2020).
- [18] R. Alert, J.-F. Joanny, and J. Casademunt, Universal scaling of active nematic turbulence, *Nat. Phys.* **16**, 682 (2020).
- [19] R. Chatterjee, N. Rana, R. A. Simha, P. Perlekar, and S. Ramaswamy, Inertia drives a flocking phase transition in viscous active fluids, *Phys. Rev. X* **11**, 031063 (2021).
- [20] S. Mukherjee, R. K. Singh, M. James, and S. S. Ray, Intermittency, fluctuations and maximal chaos in an emergent universal state of active turbulence, *Nat. Phys.* **19**, 891 (2023).
- [21] R. Großmann, P. Romanczuk, M. Bär, and L. Schimansky-Geier, Vortex arrays and mesoscale turbulence of self-propelled particles, *Phys. Rev. Lett.* **113**, 258104 (2014).
- [22] R. Großmann, P. Romanczuk, M. Bär, and L. Schimansky-Geier, Pattern formation in active particle systems due to competing alignment interactions, *Eur. Phys. J. Special Topics* **224**, 1325 (2015).
- [23] H. H. Wensink and H. Löwen, Emergent states in dense systems of active rods: From swarming to turbulence, *J. Phys. Condens. Matter* **24**, 464130 (2012).
- [24] X.-Q. Shi and H. Chaté, Self-propelled rods: Linking alignment-dominated and repulsion-dominated active matter, *arXiv:1807.00294*.
- [25] R. Mandal, P. J. Bhuyan, P. Chaudhuri, M. Rao, and C. Dasgupta, Glassy swirls of active dumbbells, *Phys. Rev. E* **96**, 042605 (2017).
- [26] K. Qi, E. Westphal, G. Gompper, and R. G. Winkler, Emergence of active turbulence in microswimmer suspensions due to active hydrodynamic stress and volume exclusion, *Commun. Phys.* **5**, 49 (2022).
- [27] A. W. Zantop and H. Stark, Emergent collective dynamics of pusher and puller squirmer rods: Swarming, clustering, and turbulence, *Soft Matter* **18**, 6179 (2022).
- [28] S. Henkes, Y. Fily, and M. C. Marchetti, Active jamming: Self-propelled soft particles at high density, *Phys. Rev. E* **84**, 040301(R) (2011).
- [29] G. Szamel, E. Flenner, and L. Berthier, Glassy dynamics of athermal self-propelled particles: Computer simulations and a nonequilibrium microscopic theory, *Phys. Rev. E* **91**, 062304 (2015).
- [30] L. Caprini and U. M. B. Marconi, Active matter at high density: Velocity distribution and kinetic temperature, *J. Chem. Phys.* **153** (2020), 184901.
- [31] L. Caprini, U. M. B. Marconi, C. Maggi, M. Paoluzzi, and A. Puglisi, Hidden velocity ordering in dense suspensions of self-propelled disks, *Phys. Rev. Res.* **2**, 023321 (2020).
- [32] S. Henkes, K. Kostanjevec, J. M. Collinson, R. Sknepnek, and E. Bertin, Dense active matter model of motion patterns in confluent cell monolayers, *Nat. Commun.* **11**, 1405 (2020).
- [33] G. Szamel and E. Flenner, Long-ranged velocity correlations in dense systems of self-propelled particles, *Europ. Lett.* **133**, 60002 (2021).
- [34] Y. Kuroda, H. Matsuyama, T. Kawasaki, and K. Miyazaki, Anomalous fluctuations in homogeneous fluid phase of active Brownian particles, *Phys. Rev. Res.* **5**, 013077 (2023).
- [35] J. Deseigne, O. Dauchot, and H. Chaté, Collective motion of vibrated polar disks, *Phys. Rev. Lett.* **105**, 098001 (2010).
- [36] B. Szabó, G. J. Szöllösi, B. Gönci, Zs. Jurányi, D. Selmeczi, and T. Vicsek, Phase transition in the collective migration of tissue cells: Experiment and model, *Phys. Rev. E* **74**, 061908 (2006).
- [37] K.-D. N. T. Lam, M. Schindler, and O. Dauchot, Self-propelled hard disks: Implicit alignment and transition to collective motion, *New J. Phys.* **17**, 113056 (2015).
- [38] F. Giavazzi, M. Paoluzzi, M. Macchi, D. Bi, G. Scita, M. L. Manning, R. Cerbino, and M. C. Marchetti, Flocking transitions in confluent tissues, *Soft Matter* **14**, 3471 (2018).
- [39] É. Fodor, C. Nardini, M. E. Cates, J. Tailleur, P. Visco, and F. van Wijland, How far from equilibrium is active matter?, *Phys. Rev. Lett.* **117**, 038103 (2016).
- [40] D. Martin, J. O’Byrne, M. E. Cates, É. Fodor, C. Nardini, J. Tailleur, and F. van Wijland, Statistical mechanics of active Ornstein-Uhlenbeck particles, *Phys. Rev. E* **103**, 032607 (2021).
- [41] Y.-E. Keta, R. L. Jack, and L. Berthier, Disordered collective motion in dense assemblies of persistent particles, *Phys. Rev. Lett.* **129**, 048002 (2022).
- [42] A. Martín-Gómez, D. Levis, A. Díaz-Guilera, and I. Pagonabarraga, Collective motion of active Brownian particles with polar alignment, *Soft Matter* **14**, 2610 (2018).
- [43] E. Sesé-Sansa, I. Pagonabarraga, and D. Levis, Velocity alignment promotes motility-induced phase separation, *Europ. Lett.* **124**, 30004 (2018).
- [44] G. Spera, C. Duclut, M. Durand, and J. Tailleur, Nematic torques in scalar active matter: When fluctuations favor polar order and persistence, *arXiv:2301.02568*.
- [45] F. D. C. Farrell, M. C. Marchetti, D. Marenduzzo, and J. Tailleur, Pattern formation in self-propelled particles with density-dependent motility, *Phys. Rev. Lett.* **108**, 248101 (2012).
- [46] Y. Fily, S. Henkes, and M. C. Marchetti, Freezing and phase separation of self-propelled disks, *Soft Matter* **10**, 2132 (2014).
- [47] See Supplemental Material at <http://link.aps.org/supplemental/10.1103/PhysRevLett.132.218301> for additional information about the movies and analysis of correlator in Fourier and real spaces.
- [48] L. Caprini, U. M. B. Marconi, and A. Puglisi, Spontaneous velocity alignment in motility-induced phase separation, *Phys. Rev. Lett.* **124**, 078001 (2020).
- [49] R. Mandal, P. J. Bhuyan, P. Chaudhuri, C. Dasgupta, and M. Rao, Extreme active matter at high densities, *Nat. Commun.* **11**, 2581 (2020).
- [50] P. Digregorio, D. Levis, A. Suma, L. F. Cugliandolo, G. Gonnella, and I. Pagonabarraga, Full phase diagram of active Brownian disks: From melting to motility-induced phase separation, *Phys. Rev. Lett.* **121**, 098003 (2018).
- [51] M. E. Cates and J. Tailleur, Motility-induced phase separation, *Annu. Rev. Condens. Matter Phys.* **6**, 219 (2015).
- [52] J.-P. Hansen and I. R. McDonald, *Theory of Simple Liquids*, 3rd ed. (Elsevier/Academic Press, Amsterdam, Boston, 2007).

- [53] M. E. Fisher, Correlation functions and the critical region of simple fluids, *J. Math. Phys. (N.Y.)* **5**, 944 (1964).
- [54] U. M. B. Marconi, L. Caprini, and A. Puglisi, Hydrodynamics of simple active liquids: The emergence of velocity correlations, *New J. Phys.* **23**, 103024 (2021).
- [55] J. L. Silverberg, M. Bierbaum, J. P. Sethna, and I. Cohen, Collective motion of humans in mosh and circle pits at heavy metal concerts, *Phys. Rev. Lett.* **110**, 228701 (2013).
- [56] J. M. Ottino, Mixing, chaotic advection, and turbulence, *Annu. Rev. Fluid Mech.* **22**, 207 (1990).
- [57] M.-C. Jullien, J. Paret, and P. Tabeling, Richardson pair dispersion in two-dimensional turbulence, *Phys. Rev. Lett.* **82**, 2872 (1999).
- [58] M. Bourgoin, Turbulent pair dispersion as a ballistic cascade phenomenology, *J. Fluid Mech.* **772**, 678 (2015).
- [59] N. T. Ouellette, E. Bodenschatz, and H. Xu, Path lengths in turbulence, *J. Stat. Phys.* **145**, 93 (2011).
- [60] H. Shiba, T. Kawasaki, and A. Onuki, Relationship between bond-breakage correlations and four-point correlations in heterogeneous glassy dynamics: Configuration changes and vibration modes, *Phys. Rev. E* **86**, 041504 (2012).
- [61] L. Varga, A. Libál, C. J. O. Reichhardt, and C. Reichhardt, Active regimes for particles on resource landscapes, *Phys. Rev. Res.* **4**, 013061 (2022).
- [62] F. Caballero and M. C. Marchetti, Activity-suppressed phase separation, *Phys. Rev. Lett.* **129**, 268002 (2022).